DESIGN OF A LONG-STROKE NONCONTACT ELECTROMAGNETIC ACTUATOR FOR

ACTIVE VIBRATION ISOLATION

Bibhuti B. Banerjee
Precision Magnetic Bearing Systems, Inc.
Cohoes, NY

Paul E. Allaire
Mechanical, Aerospace and Nuclear Engineering, University of Virginia
Charlottesville, VA

SUMMARY

A long-stroke moving coil Lorentz Actuator was designed for use in a microgravity vibration isolation experiment. The final design had a stroke of 5.08 cm (2 in) and enough force capability to isolate a mass of the order of 22.7–45.4 kg. A simple dynamic magnetic circuit analysis, using an electrical analog, was developed for the initial design of the actuator. A neodymium-iron-boron material with energy density of 278 T-kA/m (35 MGOe) was selected to supply the magnetic field. The effect of changes in the design parameters of core diameter, shell outer diameter, pole face length, and coil wire layers were investigated. An extensive three-dimensional finite element analysis was carried out to accurately determine linearity with regard to axial position of the coil and coil current levels. The actuator was constructed and tested on a universal testing machine. Example plots are shown, indicating good linearity over the stroke of approximately 5.08 cm (2 in) and a range of coil currents from -1.5 A to +1.5 A. The actuator was then used for the microgravity vibration isolation experiments, described elsewhere.

365

INTRODUCTION

A comparison of the microgravity requirements of space experiments with the actual environment available on spacecraft indicates the need for vibration isolation over a few decades in frequency [1]. While relatively high frequency disturbances may be attenuated using passive isolators, this approach fails in the very important but lower frequency regime of 0.1—10 Hz. Only active isolation at the payload-spacecraft interface with an appropriate actuator allows the synthesis of the desired isolator properties at these low frequencies and the adjustment of these properties using a control loop.

Mechanical or hydraulic actuators introduce a physical connection that may transmit undesirable vibrations and have friction and backlash [2]. Non-contacting actuators are therefore required. Among such actuators, acoustic or electrostatic types have inadequate force capabilities for realistic applications, being able to suspend masses only of the order of a few grams [2]. Electromagnetic actuators have a relatively higher force capability.

This paper discusses the design of a noncontacting electromagnetic actuator with a stroke of 5 cm (2 in) and enough force capability to isolate a mass (between 22.7 and 45.4 kg (50 and 100 lb)) connected by an umbilical to a source of low frequency vibrations. This large motion capability would provide rattle space for the isolated experiment. This rattle space is required in response to the very low frequency disturbances that may be passed on to the experiment without any attempt at isolation by the controller. The literature describes the design and use of magnetic actuators with single-stage motion capabilities of about 0.25 cm (0.1 in) or less [3, 4, 5, 6, 7]. Tandem coarse/fine schemes to overcome the small gap limitations of typical magnetic actuators and achieve isolation capabilities for very low frequency disturbances have been discussed [8, 9]. It is evident, however, that such strategies involve considerable mechanical complexity.

A single-stage long-stroke actuator with the basic advantages of a noncontacting magnetic isolation system is an attractive proposition. Force linearity with both position and current are highly desirable properties in order to simplify the feedback controller required. Moreover, in view of the ultimate goal of deployment in space, such a device has to be compact and lightweight. Power consumption and heat generation during operation—the costs associated with active control—also need to be minimized. Stroke limitations precluded the use of a moving-iron, magnetic thrust bearing-type actuator.

NOMENCLATURE

A_g, A_m	Cross-sectional area of air gap, magnet
avg	Average
B, **B**	Magnetic flux density (scalar, vector) (Tesla, T = Wb/m^2)
B_g	Radial flux density in air gap of Lorentz Actuator
B_{sat}	Saturation flux density
c, c_{cr}	Damping coefficient, critical damping coefficient
e, emf	Electromotive force (voltage)
f	Frequency (Hz)
F, $\hat{F}$	Force
F	Force (vector)
F_a	Force exerted by actuator

F_d	Direct disturbance force
F_T	Force transmitted to the base for a mass-excited system
fea	Finite element analysis
g_0	Acceleration due to gravity at sea level; 9.8 m/sec^2 (386 in/sec^2)
$G(s)$	Transfer function of plant
H	Magnetic field strength (A-turns/m)
$(-H_d, B_d)$	Magnet operating point on demagnetization curve (Appendix A)
$H(s)$	Transfer function of feedback controller
I	Current in conductor
k	Stiffness coefficient
$l, \mathbf{l}$	Length of conductor (vector $\mathbf{l} = \mathbf{l_2} - \mathbf{l_1}$)
l_g, l_m	Length of air gap, magnet
L, L_c	Inductance, inductance of (Lorentz Actuator) coil
LAMA	Long Action Magnetic Actuator
m	Mass
max, min	Maximum, minimum
n	Number of turns of current-carrying conductor
Nd-Fe-B	Neodymium iron boron (magnet material)
R_c, R_s, R_t	Resistance of (Lorentz Actuator) coil, resistance of voltage source, total resistance in Lorentz Actuator circuit ($R_t = R_c + R_s$)
$\mathfrak{R}$	Reluctance of magnetic circuit (A-turn/Wb)
s	Laplace variable ($s = j\omega$)
Sm-Co	Samarium cobalt (magnet material)
t	Time
v	Source voltage
V_g, V_m	Volume of air gap, magnet
x	Displacement (absolute) of mass (microgravity experiment) m
z_{em}	Motional electrical impedance of Lorentz Actuator ($z_{em} = \alpha^2/z_m$)
z_m	Impedance of mechanical system driven by Lorentz Actuator ($z_m = F/\dot{x}$)
α	Electromechanical coupling coefficient (or power coefficient) for a Lorentz Actuator ($\alpha = NlB_g$)
ϕ	Magnetic flux (Weber, Wb)
$\phi_c, \phi_m, \phi_{sat}$	Circuit flux, magnet flux, flux in saturated segment of magnetic circuit
η	Efficiency of electrical to mechanical power conversion by a Lorentz Actuator, as defined in Equation (4-15)
μ_0	Permeability of air ($\mu_0 = 4\pi \times 10^{-7}$ Wb/A-turn-m)
μ_r	Relative permeability of a medium
τ	Electrical time constant of the Lorentz Actuator ($\tau = L_c/R_c$)
τ_m	Equivalent mechanical time constant of the Lorentz Actuator ($\tau_m = m(R_c + R_s)/\alpha^2$)
ω_n	Natural frequency
ξ	Damping ratio

THEORY

The moving-coil-type Lorentz Actuator operates on the same principle as the voice-coil of a speaker [10]. Current is passed through a coil wound on a sleeve. The sleeve surrounds the core of the actuator and can move axially in either direction. The geometry of the actuator is shown in Figure 1. The coil is much longer than the width of the pole-face, so that the number of turns of coil wire directly underneath the pole-face in the flux path is the same for every coil position between the extremes of the stroke limit. The circumferential current flow in the coil is normal to the radial magnetic field across the pole-face gap generated by a permanent magnet in the shell of the actuator.

As shown in Figure 1 (inset), when a conductor of length $l = l_2 - l_1$ and carrying current I is placed in a magnetic field of average flux density B over the length of the conductor, a Lorentz force F is produced in a direction mutually perpendicular to both l and B:

$$\mathbf{F} = \int_{l_1}^{l_2} I(d\mathbf{l} \times \mathbf{B}) \tag{1}$$

For the Lorentz Actuator, this relation reduces to

$$F = nIlB_g = \alpha I \tag{2}$$

where $l = 2\pi r$ is the length of one turn of the coil, and the electromechanical coupling coefficient (or power coefficient) $\alpha = nlB_g$ indicates the efficiency of energy conversion for the actuator.

The motion of the coil at a velocity $\dot{x}$ in the magnetic field results in the generation of an induced voltage (a "back-emf") given by

$$e = \alpha \dot{x} \tag{3}$$

The Lorentz Actuator coil has resistance R_c and inductance L_c. The electrical circuit may be represented as in Figure 2. For this circuit, with $R_t = R_c + R_s$, and $L = L_c$, we have

$$v = L\dot{I} + R_t I + \alpha \dot{x} \tag{4}$$

The Lorentz Actuator drives a mechanical "circuit" that may be generically represented as a mass-spring-damper system. Thus, we also have

$$\alpha I = m\ddot{x} + c\dot{x} + kx \tag{5}$$

where the system is made up of a mass m, a spring of stiffness k and a damper with damping coefficient c. For microgravity vibration isolation, k and c are the umbilical stiffness and damping respectively.

Equations (4) and (5) may be used to obtain the transfer function of the Lorentz Actuator. On taking the Laplace transforms,

$$\left(Ls + R_t\right)I(s) = V(s) - \alpha sX(s)$$
$$\left(ms^2 + cs + k\right)X(s) = \alpha I(s) \tag{6}$$

Division to eliminate *I(s)* and manipulation yields the transfer function

$$\frac{X(s)}{V(s)} = \frac{\alpha}{\beta s^3 + \gamma s^2 + \delta s + \varepsilon} \tag{7}$$

where the coefficients in the denominator are

$$\beta = mL, \quad \gamma = mR_t + cL, \quad \delta = kL + cR_t + \alpha^2, \quad \varepsilon = kR_t \tag{8}$$

For this actuator, cs and k are small compared to ms^2. So, equation (7) simplifies to

$$\frac{X(s)}{V(s)} = \frac{\alpha}{s\left(mLs^2 + mR_t s + \alpha^2\right)} \tag{9}$$

Also, the electrical transients decay very rapidly, so that the electrical time constant is small and L can be neglected. Then equation (9) reduces to

$$\frac{X(s)}{V(s)} = \frac{1/\alpha}{s\left(\tau_m s + 1\right)} \tag{10}$$

where $\tau_m = mR_t / \alpha^2$ may be termed the equivalent mechanical time constant of the Lorentz Actuator. The actuator designed was used to drive a mass of 34 kg (75 lb). It was powered by a linear transconductance amplifier with a transconductance ratio of 0.5 A/V, for an effective total resistance R_t of 2 Ω (irrespective of coil resistance). Thus, the mechanical time constant for this application was $\tau_m \approx$ 19.24 sec. In contrast, the electrical time constant for the actuator was $\tau = L_c/R_c = 1.1$ milli-sec, which is negligibly small.

The electrical and mechanical system equations are coupled by the coefficient α. Strong coupling results in a high power conversion efficiency η, given by

$$\eta = \frac{\alpha I\dot{x} - c\dot{x}^2}{\alpha I\dot{x} + R_t I^2} \tag{11}$$

Nonlinearity in a Lorentz Actuator is primarily caused by the coil moving out of the uniform magnetic field in the air gap as its position varies over the entire stroke. This results in the electromechanical coupling coefficient becoming a nonlinear function of displacement, instead of being a constant. In addition, if a voltage source is used to power the Lorentz Actuator, Equations (4) and (5) take nonlinear forms given by

$$v = L\dot{I}(x) + R_tI(x) + \alpha(x)\dot{x}$$
$$\alpha(x)I(x) = m\ddot{x} + c\dot{x} + kx$$

(12)

For the Lorentz Actuator designed, the use of a long coil length and of current feedback ensures good linearity. A longer coil length, however, also results in an increased inductance and a higher electrical time constant for the actuator.

INITIAL DESIGN

While the main reason to pick the Lorentz Actuator over an actuator like a magnetic thrust bearing is the much longer stroke capability possible, there are other advantages too. Unlike the magnetic bearing, it is open-loop and neutrally stable, thus eliminating the need for a redundant control system and backup power supply. Nor is a constant bias current necessary for steady state operation, so that the power requirements under these conditions are very small. The linearity offered by a Lorentz Actuator greatly simplifies control system design and operation. The relatively low force capability is not an issue for microgravity applications, since the forces required are quite small (of the order of one pound).

The initial design was developed using the basic techniques of linear magnetic circuit analysis. Neodymium iron boron (Nd-Fe-B), with a high maximum energy product of 278 T-kA/m (35 MGOe), was chosen as the magnet material[1]. This commercially available material has the composition $Nd_{15}Fe_{77}B_8$. This choice was dictated by the need for a compact actuator which would nonetheless exhibit a linear force-vs.-current trend. Samarium cobalt (Sm-Co) was also considered, but a comparison showed that the magnetic and mechanical properties of Nd-Fe-B are superior because of its iron content. Nd-Fe-B is 15% lighter, which is significant for a space application, and cheaper. The two areas of advantage for Sm-Co—relative inertness and better thermal stability—were not of much importance here.

Fringing and leakage of the magnetic field were not modeled, but an attempt to minimize their deleterious effects was made by applying a rule of thumb that requires the gap ratio—the ratio of the shell-to-core gap to the pole-face gap—to be about 3:1 or higher. A design algorithm was developed to carry out the Lorentz Actuator design [12].

Some observations on sizing the magnet may be made. For a magnet of length l_m and cross-sectional area A_m operating at the point $(-H_d, B_d)$ on its normal demagnetization curve [12] and producing a flux density B_g in an air gap of length l_g and cross-sectional area A_g in a typical Lorentz Actuator geometry, we have

$$B_gA_g = B_dA_m$$

(13)

and

$$H_dl_m = -\frac{B_g}{\mu_0}l_g$$

(14)

---

[1]Crumax® 355, a product of Crucible Magnetics, Crucible Materials Corporation, 101 Magnet Drive, Elizabethtown, Kentucky 42701.

Here, μ_0 is the permeability of air, and the reluctance of the iron path is assumed to be negligible compared to that of the air gap. Multiplying these two equations and rearranging gives us

$$B_g^2 = -\mu_0 (B_d H_d) (V_m / V_g) \tag{15}$$

where the volumes of the magnet and the air gap are represented, respectively, by $V_m = A_m l_m$ and $V_g = A_g l_g$. A greater volume of magnet material can thus result in a higher value of the air gap flux density, provided the same energy product $(B_d H_d)$ is maintained. Generally, changing either the length l_m or the cross-section A_m of the magnet to change the volume of the magnet results in changing the operating point of the magnet on the demagnetization curve, so that the energy product is also changed. Dividing Equation (13) by (14) yields the slope of the load-line:

$$\frac{B_d}{\mu_0 H_d} = -\frac{l_m}{A_m} \frac{A_g}{l_g} \tag{16}$$

An increase in the length of the magnet must be accompanied by a corresponding increase in its cross-sectional area, or vice-versa, so as to maintain the same slope of the load-line. In effect, this does not change the operating point, so that the energy product also stays the same, even though the volume of the magnet has increased.

It was found that a reduction of the core diameter helped to improve position linearity. While increasing the axial length of the air gap by axially elongating the pole-face helped improve the gap flux density and actuator force, imparting a "lip" to the actuator enhanced position linearity. The magnet protrudes radially outside the pole-piece and the base, reducing the leakage factor significantly [13].

A number of design iterations were carried out for a circuit of magnet iron, with a saturation flux density, B_{sat} of 1.2 T (Tesla). The Nd-Fe-B magnet required for the resulting design could not be made in one piece—the large outer diameter (8.13 cm (3.20 in)) would require it to be made up of sectors. It was decided to analyze this design using finite elements.

FINITE ELEMENT ANALYSIS

An effort was made to try to come up with a more compact design, within a constraint of 5.08 cm (2 in) as the outer diameter of the magnet, this dimension being the manufacturer's limit for a one-piece Nd-Fe-B magnet. It was hypothesized that a reduction of the core diameter to saturate the core would enable us to satisfy this constraint, with its concomitant reduction in the magnet diameter. This would deliberately violate the rule of thumb about the minimum gap ratio required, and yet minimize flux leakage and its consequent nonlinearity problem, since a magnetic material, when saturated, has the permeability of air. Finite element analysis [14] was used in this context to produce a better design.

A detailed finite element analysis enabled the realistic consideration of flux leakage and fringing effects. The effect of magnetic saturation of part of the circuit could be studied, as also that of using different geometric configurations to minimize weight and cost. Properties of magnetic materials were input as B-H tables, so that operation in the nonlinear region of a material's B-H curve was permitted.

The model also included the effect of change in the air gap flux due to the varying magnetic flux associated with changing coil current.

A finite element analysis package[2] suitable for solving a three-dimensional axisymmetric problem on a personal computer was used. The initial design of the Lorentz Actuator, as specified in the last section, was then modeled. The amount of flux leakage observed was judged high enough to cause unacceptable variations in force with changes in position of the coil.

A number of designs, incorporating a constraint of 4.95 cm (1.95 in) (to allow for machining losses with a 5.08 cm (2 in) cylindrical ingot, the largest available) on the outer diameter of the magnet, were analyzed by this technique. The finite element mesh consisted predominantly of quad elements, though some triangular ones were also used. The mesh used for the final design is shown in Figure 3, along with a typical flux plot (Lorentz Actuator final design, coil in its innermost position carrying a current of 2.5 A (into the plane of the page)). A total of 499 elements made up the axisymmetric finite-element model, with the air gap and shell-to-core gap regions being very finely meshed into 162 elements.

The generation of the required force while maintaining linearity, with respect to both coil position and coil current, and compactness is the crux of the problem. Position linearity requires that, for a constant coil current, the actuator force remain the same irrespective of the axial position of coil, within the stroke bounds. On the other hand, current linearity at a given coil position calls for the actuator force to vary linearly with changes in the coil current between its upper and lower design limits. Current linearity, therefore, requires that the average flux density across the effective air gap remain constant with variations of the coil current. The effective air gap is generally longer (in the axial direction) than the air gap radially beneath the pole-face due to flux leakage.

The design iterations were driven by the conflicting needs of satisfying the force requirement and maintaining linearity. While the limit on the outer diameter of the magnet provided the design envelope in the radial direction, the total stroke of 5.08 cm (2 in) dictated that the coil be considerably more than 5.08 cm (2 in) long to ensure that the same number of turns of the coil "cut" the effective air gap. This helped ensure force linearity with position from one end of the stroke to the other. The thickness of the air gap depended on a compromise between reducing it to decrease the circuit reluctance so as obtain increased flux density and force, and increasing it to accommodate a greater number of (radial) layers of coil wire (of the same gage) in order to increase the force.

FINAL DESIGN

The final design, obtained after a number of iterations with the finite element model, is shown in Figure 4. The magnetic material used for the circuit was a nickel-iron alloy with 48% nickel content[3]. In bar form, this material exhibits very high permeability and nominally saturates at approximately 1.5 T. A coil current density of 155 A/cm^2 (1000 A/in^2) was picked for continuous use to ensure cool operation, even though a fivefold increase in the current density is possible for peak loads. Other design data for this actuator, which was built and tested, are provided in Table 1.

The results obtained by finite element analysis indicated that this design would have a high degree of position and current linearity. The predictions and actual measurements are presented in the following section.

TEST RESULTS

A universal testing machine was used to test the Lorentz Actuator for load capacity at various coil positions and coil currents. Because of thermal considerations, currents of up to ±1.5 A only were tested. The resulting data were then analyzed and compared with the predictions based on finite element analysis. These results are presented in Figure 5 for positive coil currents. Almost identical results for negative coil currents are not presented here for the sake of brevity.

The motivation for this figure is to check for position linearity. Least squares fitting of a regression line has been carried out for each set of experimental data. The slope of each of these regression lines would have been zero for perfect position linearity. A small amount of leakage flux exists in the air between axial distances of 0.76 cm (0.3 in) and 5.84 cm (2.3 in), even though this was neglected in the predictions. Furthermore, the tolerance of 0.13 mm (5 mils) for the magnet inner diameter was a compromise between the requirements of accuracy and cost. Combined with unknown inaccuracies introduced during the vendor's assembly procedure, it resulted in more flux leakage than expected from finite element analysis. (This is corroborated by the analysis of flux measurements, which follows). As the coil moves further towards the closed end, more turns of the coil "cut" this leakage flux, so that the magnitude of the force increases. Since the coil length has been chosen to take advantage of the fringing flux at the open end even at the innermost position of the coil, there is no corresponding reduction on this account with inward coil motion.

The next figure, Figure 6, presents the data from the perspective of current linearity. Again, linear regression lines have been fitted to the experimentally obtained data, revealing that the current linearity observed is very good (note the extremely good correlation). The higher slope of the least square line compared to the predicted results line is indicative of higher forces in each case than predicted, again because of the reasons mentioned earlier. Also, as expected from the discussion for position linearity in the previous paragraph, the slope of the least square line increases as the coil moves inward.

A gaussmeter was used to measure the radial flux density in the air gap over an axial travel of 2.03 cm (0.8 in) to 11.43 cm (4.5 in) from the base. Flux densities were measured along axial lines at 45 ° intervals circumferentially around the annular air gap, using a probe of 0.25 mm (10 mils) thickness. The unbroken line ("avg") in Figure 7 represents the average of each set of eight values observed at a particular axial distance. The values observed in the pole-face region are lower than predicted by finite element analysis (dashed line "fea"), but spread out over a longer axial length. The "error bars" along this line represent the spread between the maximum and minimum values observed at the corresponding points. The fact that this spread is much higher in the shell-to-core region than elsewhere is attributable to inaccuracies in machining and assembly mentioned earlier.

An error analysis was performed to verify that the differences between the measured and predicted flux over the pole-face gap were within the limits resulting from dimensional and magnetic tolerances. The analysis predicted an error of ±5.64% in the magnetic flux in this region. The actual error over this range was calculated to be −3.83%, well within the predicted limits [12].

CONCLUSION

The theory for the design of a long-stroke electromagnetic actuator for space vibration isolation has been presented. A preliminary design was verified and optimized using finite element analysis. The actuator was then constructed and tested for load capacity and gap flux. It exhibited excellent force linearity with respect to position and current.

This actuator was used in an actively controlled vibration isolation testbed in the laboratory where both springs and an air dashpot were used as umbilicals. Reduction ratios of 40 dB or greater were achieved, as desired, in each case tested [12, 15].

REFERENCES

[1]   Nelson, E. S., "An Examination of Anticipated g-Jitter on Space Station and Its Effect on Materials Processes," *NASA TM–103775*, April 1991.

[2]   Naumann, R. J. and D. D. Elleman, "Containerless Processing Technology," *Materials Sciences in Space*, Ed. B. Feuerbacher, Springer Verlag, Berlin, 1986.

[3]   Owen, R. G. and D. I. Jones, "Columbus Applications Study (WP. 1.1)," Technical Note No. BTN 001, University College of North Wales, School of Electronic Engineering Science, Bangor, Gwynedd, Sep. 1988.

[4]   Havenhill, D. D. and K. D. Kral, "Payload Isolation Using Magnetic Suspension," AAS 85 014, *Annual AAS Guidance and Control Conference*, Keystone, Colorado, Feb. 2–6, 1985.

[5]   Allen, T. S., D. D. Havenhill and K. D. Kral, "FEAMIS: A Magnetically Suspended Isolation System for Space Based Materials Processing," AAS 86 017, *Annual AAS Guidance and Control Conference*, Keystone, Colorado, Feb. 1–5, 1986.

[6]   Hibble, W., P. J. Wolke and M. Smith, "A Magnetic Isolation and Pointing System for the Astrometric Telescope Facility," *Workshop on Magnetic Suspension Technology*, NASA Langley, Hampton, Virginia, Feb. 2–4, 1988.

[7]   Jones, D. I., A. R. Owens, R. G. Owen and G. Roberts, "Microgravity Isolation Mount: Design Report," Technical Note BTN 009, University College of North Wales, School of Electronic Engineering Science, Bangor, Gwynedd, Sep. 1989.

[8]   Hamilton, B. J., J. H. Andrus and D. R. Carter, "Pointing Mount with Active Vibration Isolation for Large Payloads," AAS 87 033, *Annual AAS Guidance and Control Conference*, Keystone, Colorado, Jan. 31–Feb. 4, 1987.

[9]   Allan, A. P. and C. R. Knospe, "A Six Degree-of-Freedom Magnetic Bearing for Microgravity Vibration Isolation," *International Symposium on Magnetic Suspension Technology*, NASA Langley, Hampton, Virginia, August 1991.

[10]   Carlson, A. B., D. G. Gisser and F. K. Manasse, "Magnetics and Electromechanics," Chapter 17, *Electrical Engineering: Concepts and Applications*, Addison Wesley Publishing Company, Reading, Massachusetts, 1989.

[11]   Olson, H. F., *Solution of Engineering Problems by Dynamical Analogies*, Second Edition, D. Van Nostrand, Princeton, New Jersey, 1966.

[12]   Banerjee, B. B., "Active Vibration Isolation of Microgravity Experiments with Umbilicals Using Magnetic Actuators," Ph. D. Dissertation, Univ. of Virginia, Charlottesville, May 1994.

[13]   McCaig, M. and A. G. Clegg, *Permanent Magnets in Theory and Practice*, John Wiley & Sons, New York, 1987.

[14]   Allaire, P. E., *Basics of the Finite Element Method*, Wm. C. Brown Publishers, 1985.

[15]   Banerjee, B. B., Allaire, P. E., and Grodsinsky, C. M., "Active Vibration Isolation of Microgravity Experiments with Spring Umbilicals Using an Electrodynamic Actuator," 3rd. International Symposium on Magnetic Suspension Technology, NASA CP-   , 1995.
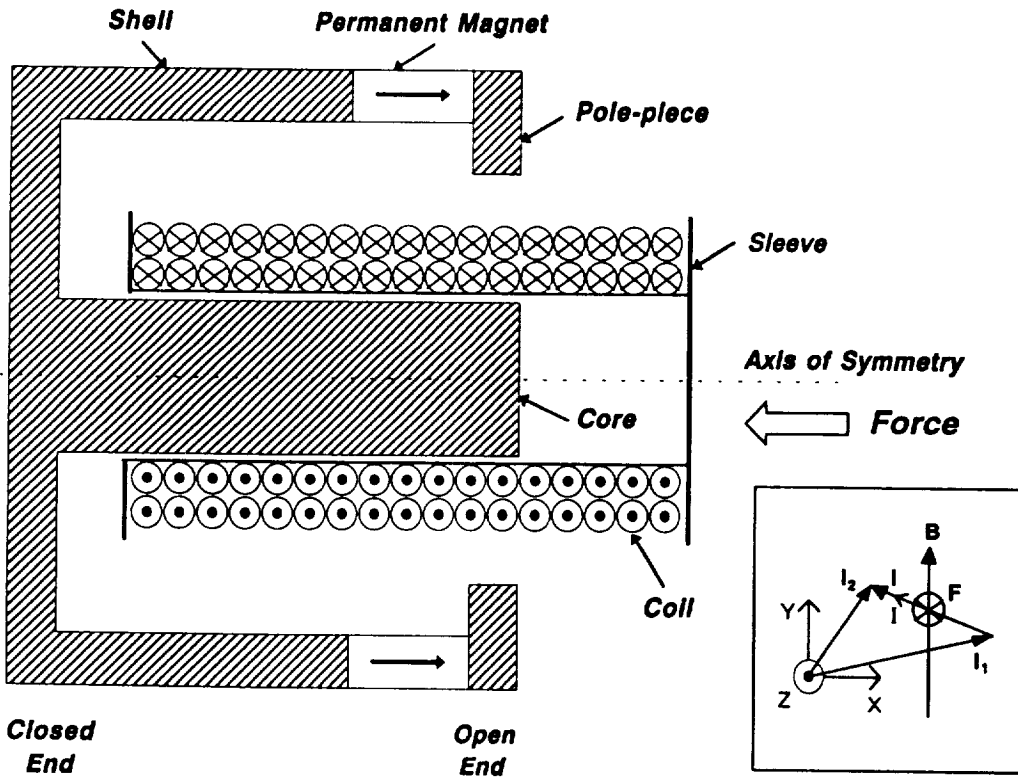
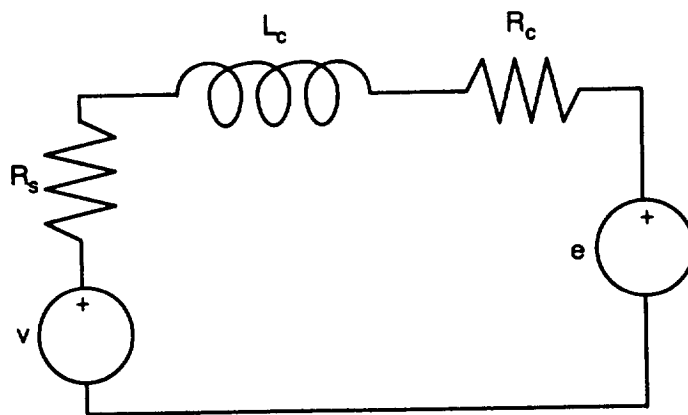Figure 1. Cross-Section of a Lorentz Actuator (Not to Scale) and the Lorentz Force on a Conductor in a Magnetic Field (Inset)

Figure 2. Electrical Circuit for Lorentz Actuator

MODEL: NL21N   CASE:

MAGNETIC FLUX DENSITY (TESLAS)
MAXIMUM = 1.580
    1.580
    1.459
    1.338
    1.216
    1.095
    0.9737
    0.8523
    0.7310
    0.6096
    0.4803
    0.3669
    0.2456
    0.1243
    0.2989E-02
MINIMUM = 0.2989E-02
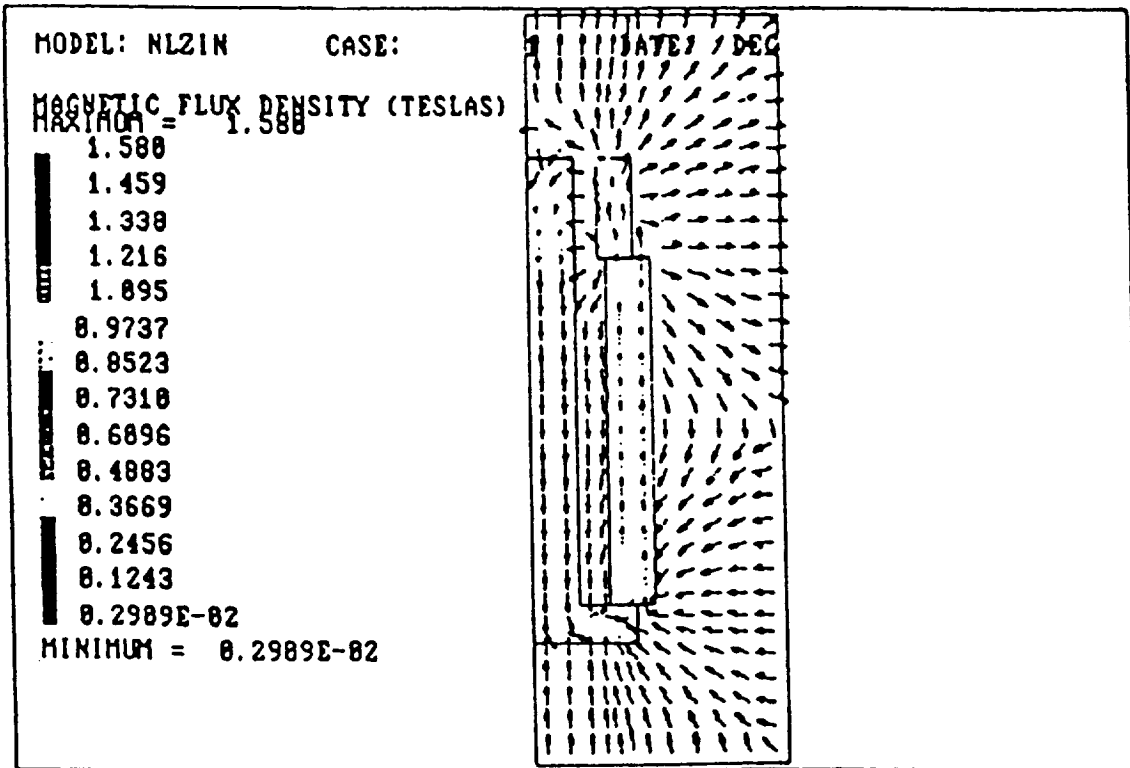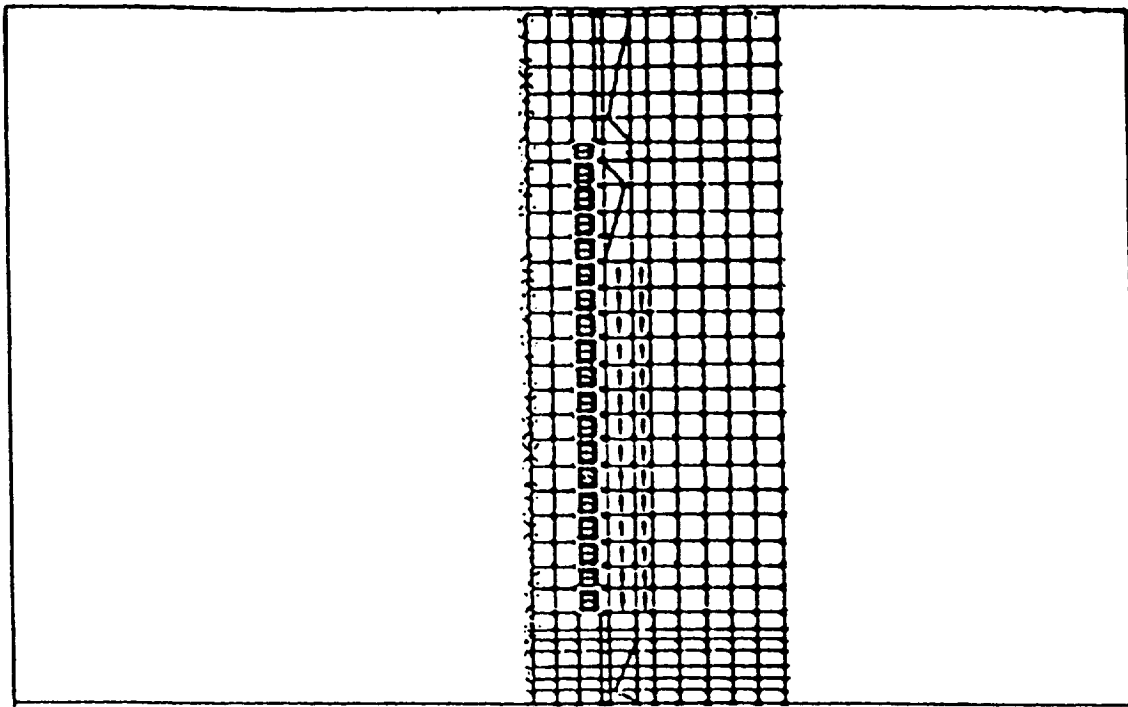
Figure 3. Finite Element Mesh for the Lorentz Actuator (Top Half of an Axisymmetric Cross-Section, with Air Elements Surrounding it) and Flux Plot for Coil at 0.3 in (0.76 cm), Current = +2.5 A
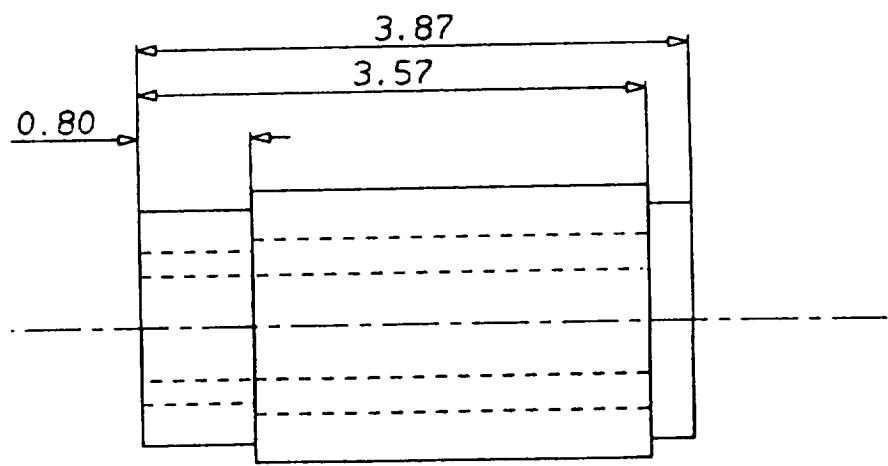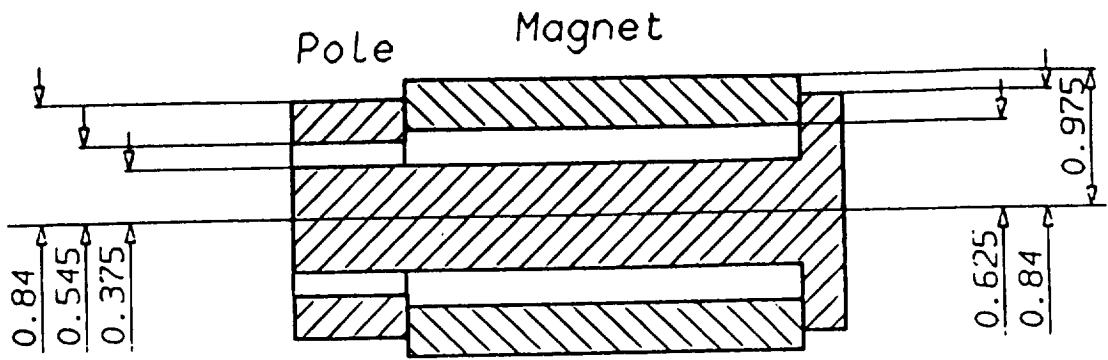
Figure 4. Lorentz Actuator: Final Design
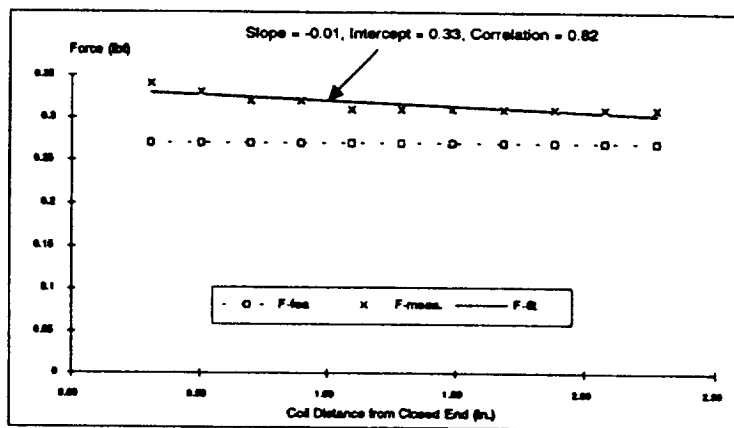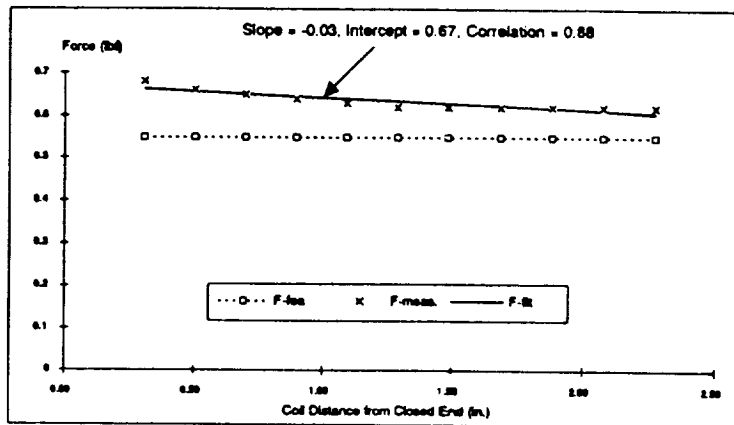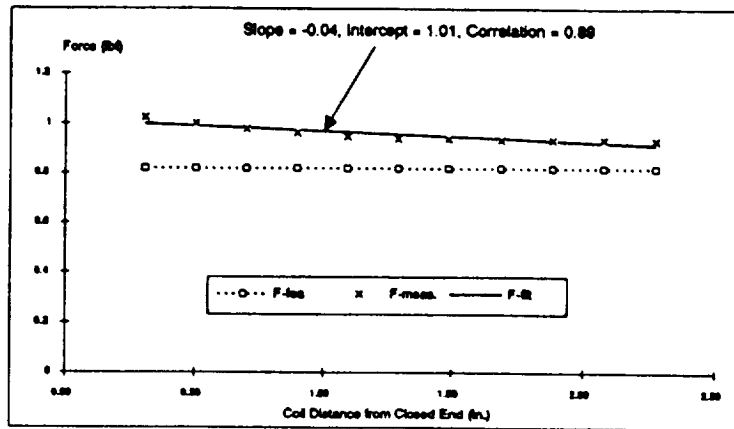
Figure 5. Position Linearity: Measured and Predicted Forces for Positive Coil Currents (I = 1.5A, 1.0A & 0.5A respectively, starting at the top)
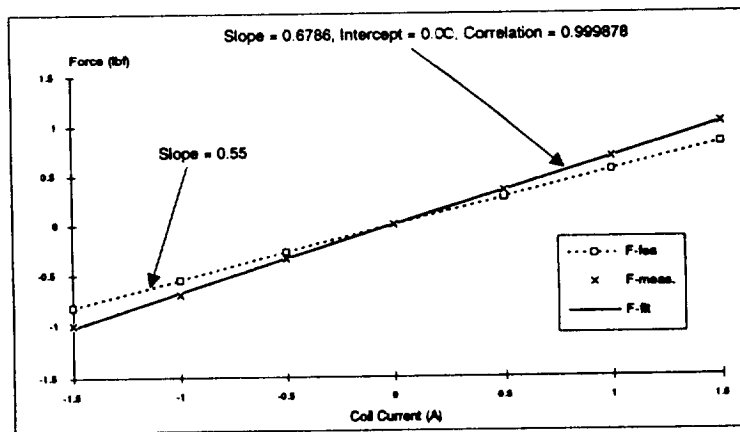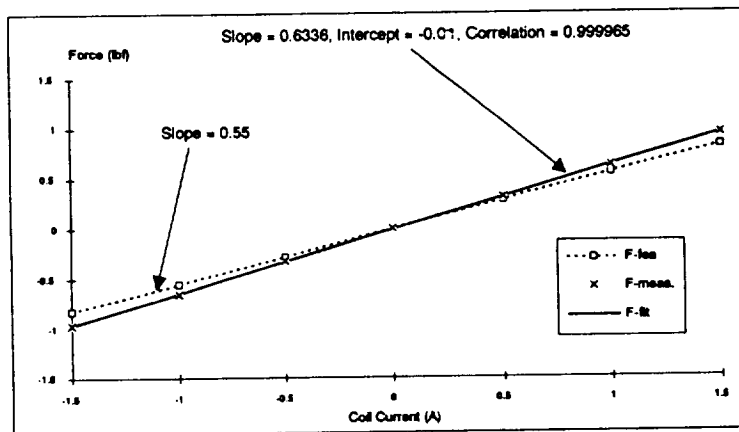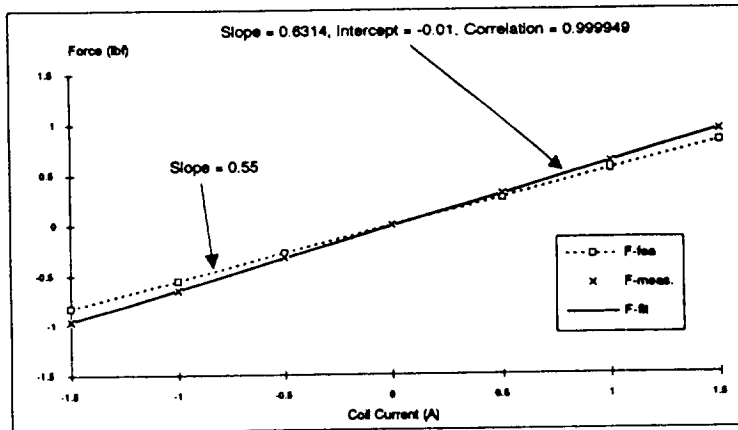
Figure 6. Current Linearity: Measured and Predicted Forces for Three Coil Positions ('out,' 'mid' and 'in' respectively, starting at the top)
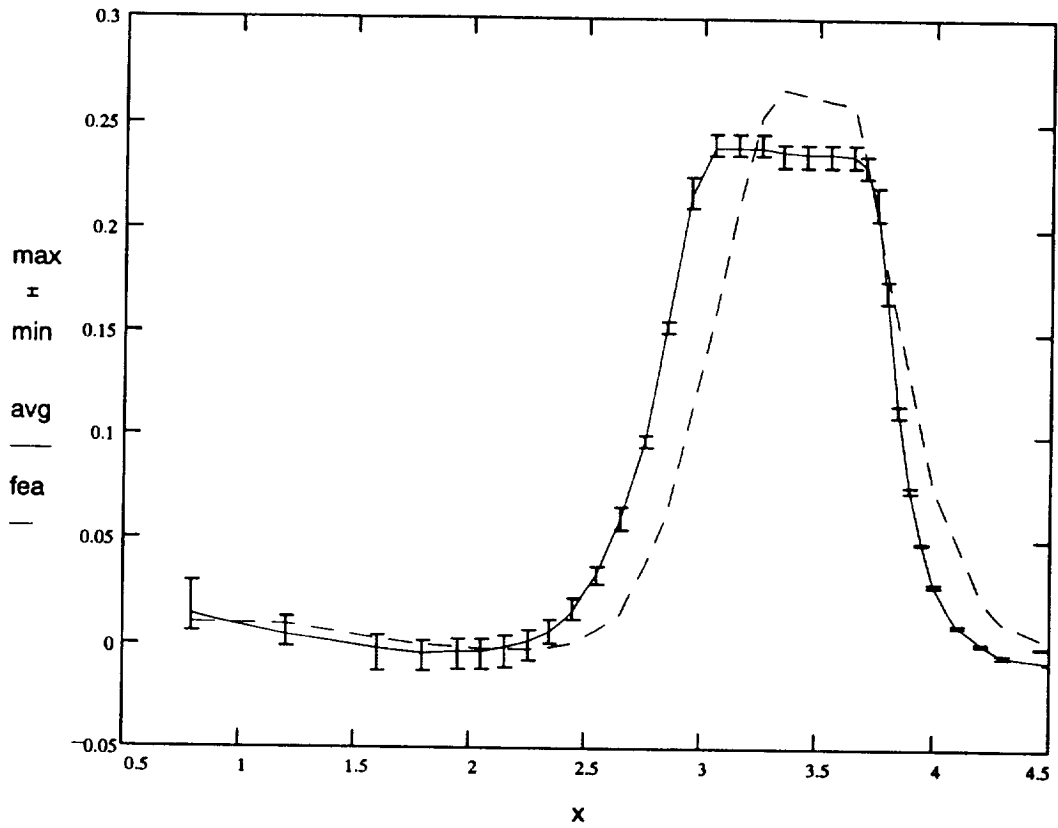
Figure 7. Radial Flux Density (Tesla) vs. Axial Distance (inches, from Closed End) in Lorentz Actuator Air Gaps (Current in Coil = 0 A)

Table 1. Lorentz Actuator: Final Design Specifications

Total length	9.83 cm (3.87 in)
Magnet outer diameter	4.95 cm (1.95 in)
Magnet inner diameter	3.18 cm (1.25 in)
Magnet length	7.04 cm (2.77 in)
Shell outer diameter	4.27 cm (1.68 in)
Shell base length	0.76 cm (0.30 in)
Pole-face length	2.03 cm (0.80 in)
Core diameter	1.90 cm (0.75 in)
Air gap	0.43 cm (0.17 in)
Shell-to-core gap	0.64 cm (0.25 in)
Gap ratio	1.47 : 1
Axial length of coil	10.16 cm (4 in)
Wire (#22, 130°C) diameter	0.68 mm (26.7 mils)
Total number of turns	150 x 4
Coil resistance (measured)	2.7 Ω
Inductance (measured, fully in)	3 mH
Maximum coil current	2.5 A
Air gap flux density (average)	0.2135 T
Maximum force generated	5.56 N (1.25 lbf)
Theoretical power coefficient	1.88 N/A (0.42 lbf/A)
Actual power coefficient	2.22 N/A (0.50 lbf/A)
Actuator weight (excl. coil)	1.03 kg (2.28 lb)

-

REPORT DOCUMENTATION PAGE

| 1. AGENCY USE ONLY (Leave blank) | 2. REPORT DATE
July 1996 | 3. REPORT TYPE AND DATES COVERED
Conference Publication |
|---|---|---|

4. TITLE AND SUBTITLE

Third International Symposium on Magnetic Suspension Technology

5. FUNDING NUMBERS

WU 505-64-70-03

6. AUTHOR(S)

Nelson J. Groom and Colin P. Britcher, Editors

7. PERFORMING ORGANIZATION NAME(S) AND ADDRESS(ES)

NASA Langley Research Center
Hampton, VA 23681-0001

8. PERFORMING ORGANIZATION REPORT NUMBER

L-17591A

9. SPONSORING/MONITORING AGENCY NAME(S) AND ADDRESS(ES)

National Aeronautics and Space Administration
Washington, DC 20546-0001

10. SPONSORING/MONITORING AGENCY REPORT NUMBER

NASA CP-3336
Part 1

11. SUPPLEMENTARY NOTES

Nelson J. Groom: Langley Research Center, Hampton, VA; Colin P. Britcher: Old Dominion University, Norfolk, VA

12a. DISTRIBUTION/AVAILABILITY STATEMENT

Unclassified–Unlimited
Subject Category 18
Availability: NASA CASI (301) 621-0390

12b. DISTRIBUTION CODE

13. ABSTRACT (Maximum 200 words)

In order to examine the state of technology of all areas of magnetic suspension and to review recent developments in sensors, controls, superconducting magnet technology, and design/implementation practices, the Third International Symposium on Magnetic Suspension Technology was held at the Holiday Inn Capital Plaza in Tallahassee, Florida on December 13–15, 1995.

The symposium included 19 sessions in which a total of 55 papers were presented. The technical sessions covered the areas of bearings, superconductivity, vibration isolation, maglev, controls, space applications, general applications, bearing/actuator design, modeling, precision applications, electromagnetic launch and hypersonic maglev, applications of superconductivity, and sensors. A list of attendees appears on page xv of the document.

14. SUBJECT TERMS

Magnetic bearings; Magnetic suspension; Large gap magnetic suspension; Small gap magnetic suspension; Maglev; Sensors; Superconducting magnetic suspension systems; Control systems

15. NUMBER OF PAGES
407

16. PRICE CODE
A18

| 17. SECURITY CLASSIFICATION OF REPORT
Unclassified | 18. SECURITY CLASSIFICATION OF THIS PAGE
Unclassified | 19. SECURITY CLASSIFICATION OF ABSTRACT
Unclassified | 20. LIMITATION OF ABSTRACT |
|---|---|---|---|